Supporting Information: Phase-Separated Nanophotonic Structures by Inkjet Printing

Yidenekachew J. Donie,[*,†] Stefan Schlisske,[†,‡] Radwanul H. Siddique,[¶,§] Adrian Mertens,[†,‖] Vinayak Narasimhan,[§] Fabian Schackmar,[†,‡,‖] Manuel Pietsch,[†,‡] Ihteaz M. Hossain,[†,‖] Gerardo Hernandez-Sosa,[†,‡] Uli Lemmer,[*,†,‡,‖] and Guillaume Gomard[*,†,‖]

†*Light Technology Institute, Karlsruhe Institute of Technology, Engesserstr. 13, 76131 Karlsruhe, Germany.*

‡*InnovationLab, Speyerer Str. 4, 69115 Heidelberg.*

¶*Image Sensor Lab, Samsung Semiconductor, Inc.,2 N Lake Ave. Ste. 240, Pasadena, California 91101, USA.*

§*Medical Engineering, California Institute of Technology (Caltech), 1200 E. California Blvd, Pasadena, California 91125, USA.*

‖*Institute of Microstructure Technology, Karlsruhe Institute of Technology, Hermann-von-Helmholtz-Platz 1, 76344 Eggenstein-Leopoldshafen, Germany.*

E-mail: yidenekachew.donie@kit.edu; ulrich.lemmer@kit.edu; guillaume.gomard@zeiss.com

Phase-separation in polymer blend inks

To monitor the phase separation process prior to printing, inks with concentration varying between 50 and 300 mg.ml^{-1} were prepared and heated at 80 °C to completely dissolve the polymers in the solvent and to then obtain a transparent (or clear) solution. Afterward, the change in the transparency of the solution (which is an indication of phase separation[1–3]) was monitored for six weeks but no change in transparency was observed for the tested inks (see the photograph of the solutions after six weeks in **Figure S1**a-d).

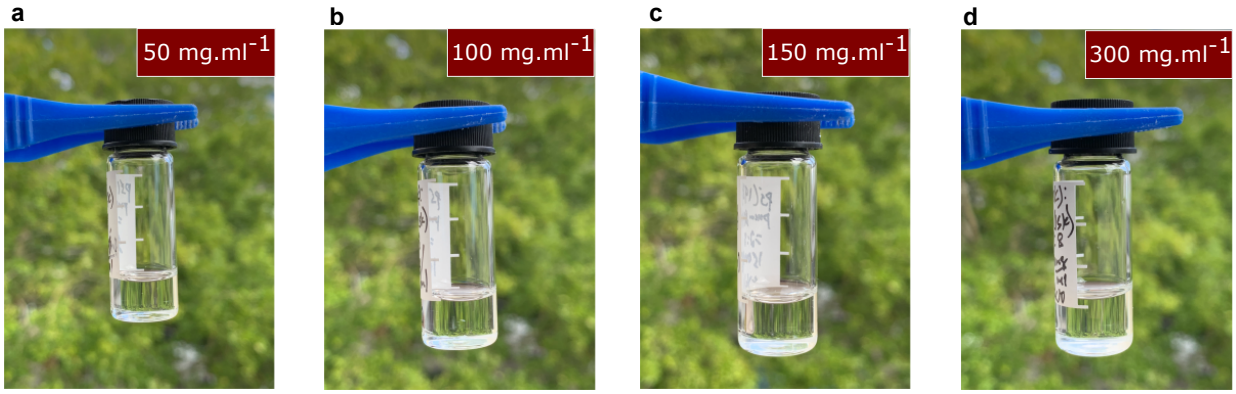

Figure S1. Monitoring the transparency of polymer blend inks with different concentration. Photographs of polymer blend after six weeks, with a concentration of (a) 50 mg.ml^{-1}, (b) 100 mg.ml^{-1}, (c) 150 mg.ml^{-1} and (d) 300 mg.ml^{-1}.

Inkjet-printed phase-separated nanostructures at room temperature

It was found that PS:PMMA inks based on co-solvents (cyclohexanone and tetralin in 90:10 volume ratio) lead to PSNs initiated by the solvent extraction at room temperature upon IJP, as shown in **Figure S2**a,b. This finding offers the opportunity to IJP temperature sensitive materials such as biopolymers. The printed films are however inhomogeneous, regardless of the printing parameters or of the ink formulation we considered. The most probable explanation is the non-uniform drying of the printed films caused by the limited number of used nozzles, 16 in the present case. Thus, to obtain more uniform films at room temperature, it would be necessary to increase the number of nozzles to decrease the

drying rate of the ink before diffusing into the film. The photographs of pixels printed at a substrate temperature of 25 °C on silicon and on glass are shown in **Figure S2** along with the corresponding microscopy images of the PSNs. The morphology of the resulting

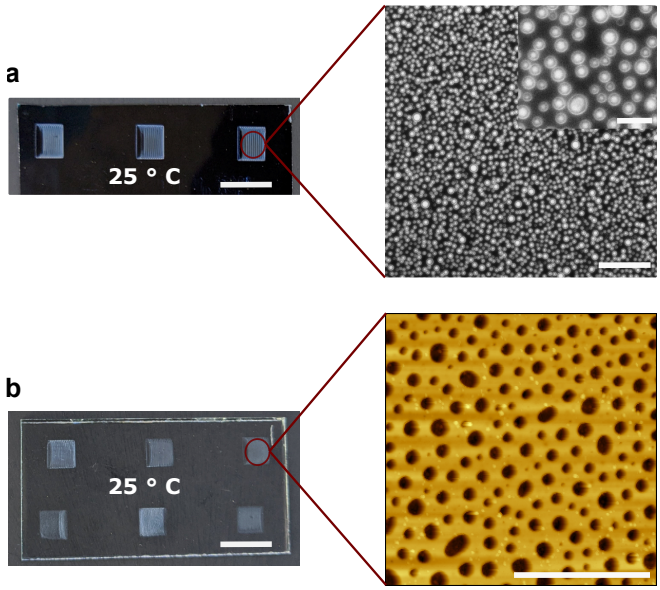

Figure S2. Inkjet-printing of PS:PMMA (30:70) ink with bi-directional printing direction at a substrate temperature of 25 °C. Photographs of PMMA matrix (average thickness of 150 nm) after selective development of PS domains. Printing on (a) a silicon substrate and (b) a glass substrate. The scale bar in the photograph of the substrates represent 1 cm. The main scale bar in the AFM and SEM images represent 5 μm, and 2 μm for the inset SEM image in (a).

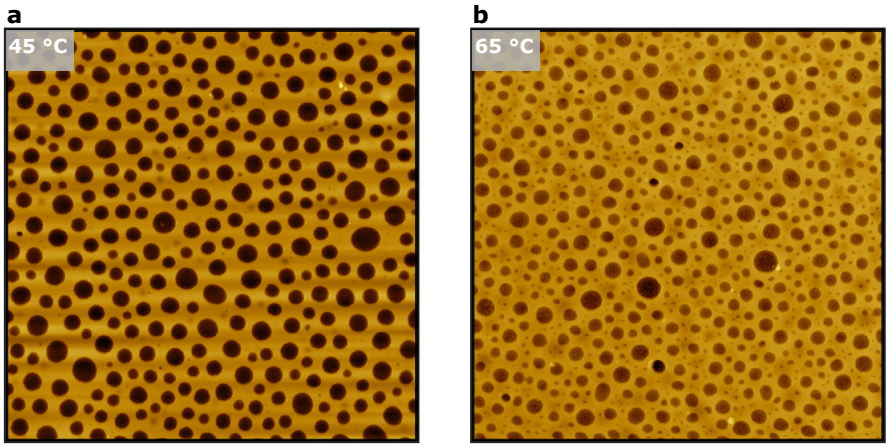

Figure S3. Inkjet-printing of PS:PMMA (30:70) ink with different substrate temperatures. The AFM images (5 μm $\times$ 5 μm) of the sample prepared with a substrate temperature of (a) 45 °C and (b) 65 °C.

PSNs can be tuned by adjusting the temperature of the printing table supporting the glass substrates. Finer domains are observed at a higher printing table temperature (see **Figure S3**). This might be attributed to the increase of the common solvent's evaporation rate with the substrate temperature rise, which reduces the time available for the phase separated domains to coalesce into larger ones.[4]

Phase diagram of a polymer blend of PS and PMMA

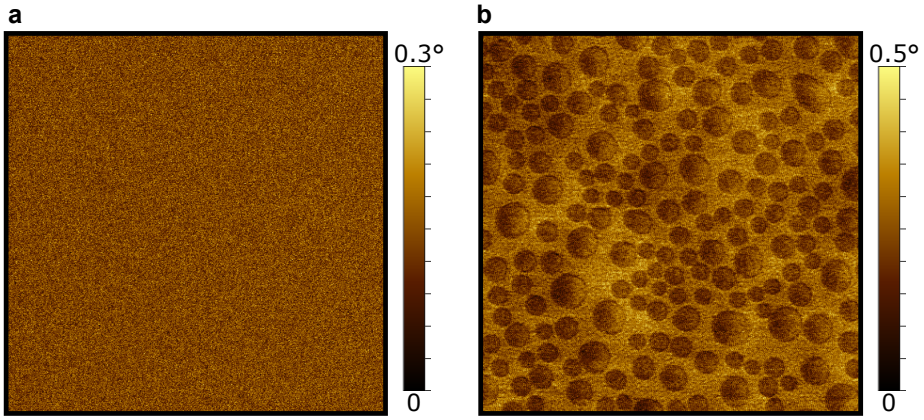

Figure S4. AFM topographic images (8 μm $\times$ 8 μm) of printed PS:PMMA films. Phase image of the film (a) pre-annealing and (b) post-annealing at temperature of 250°C. In (b) the dark areas (PS) represent regions with a low phase shift, and the light areas possess a much higher phase shift and they represent the PMMA polymer matrix.

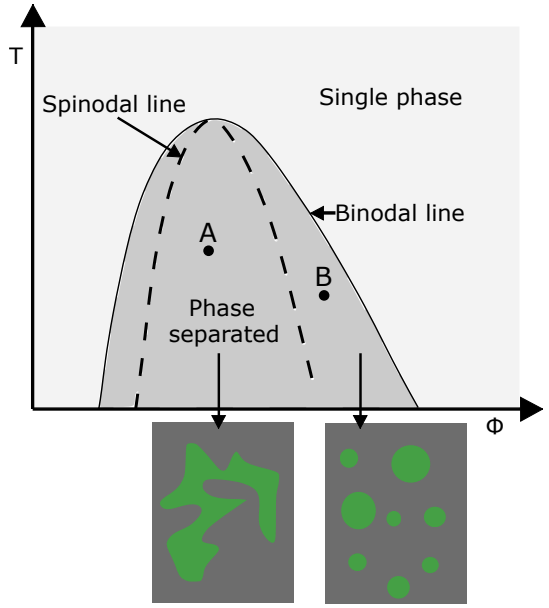

Figure S5. Schematic phase diagram of a polymer blend of PS and PMMA as a function of weight ratio of PMMA, ϕ and temperature, T. Above the binodal line, the system is a one-phase mixture. Below, the binodal line, the mixture separates into PS and PMMA phases. Between the binodal and spinodal (dashed) line at B, the phase separation happens *via* nucleation and growth. Outside of the nucleation and growth region (A) phase separation occurs *via* spinodal decomposition and leads to disordered bicontinuous network (tortuous channels). Adapted from Ref.[5]

Inkjet-printing of phase-separated nanostructures on silicon substrates

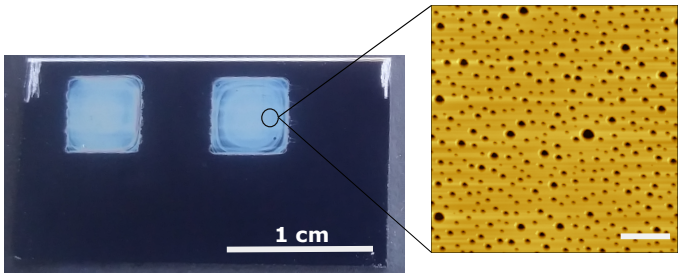

Figure S6. Inkjet-printing of PSNs on a silicon substrate (ink based on PS:PMMA (20:80)). Photographs of PMMA matrix (average thickness of 150 nm) obtained after annealing the printed ink at 200 °C for 5 min and after the selective development of PS. The scale bar in the corresponding AFM image represents 2 μm.

Influence of the polymer blend composition on the resulting PSNs diameter size distribution

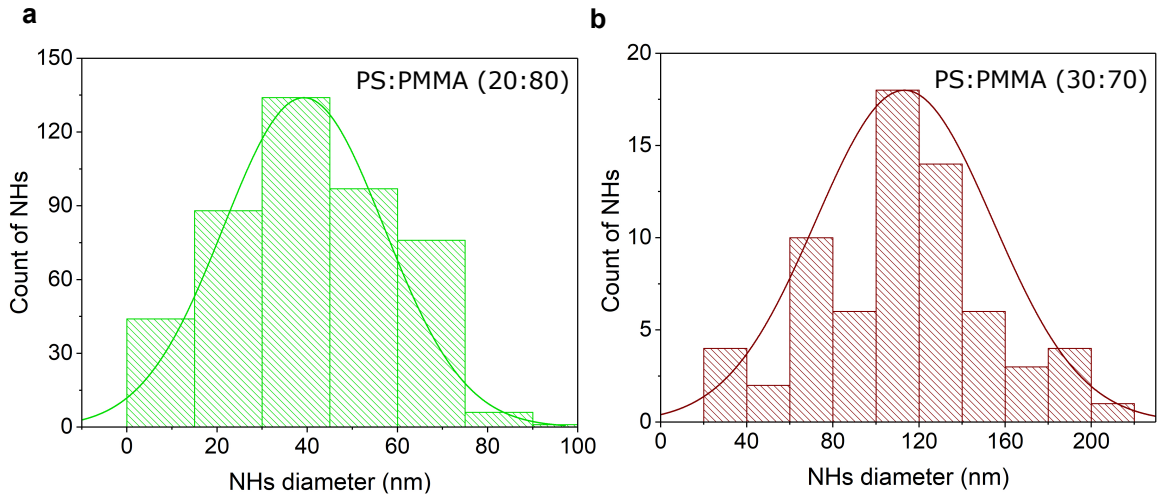

Figure S7. Size analysis of the disordered NH array for different weight ratios of PS:PMMA. A Gaussian distribution with a mean hole diameter of (a) 40 nm, and (b) 113 nm is obtained for inks with a PS:PMMA weight ratio of 20:80 and 30:70, respectively, and after annealing at 150 °C for 5 min and after the selective development of the PS phase. The solid lines in (a) and (b) represent the Gaussian fit.

Influence of the annealing temperature on the morphology of the printed PSNs

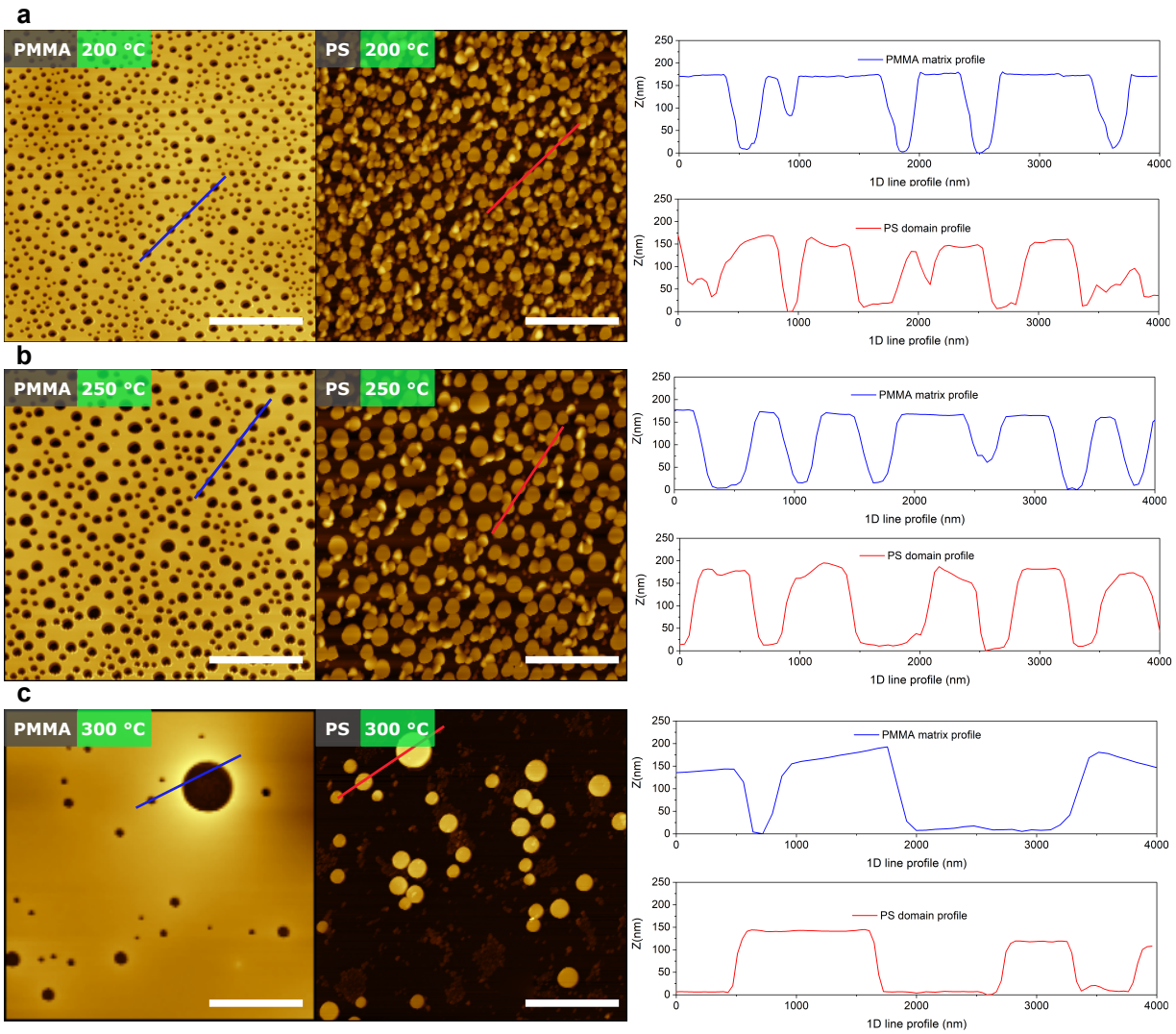

Figure S8. Influence of the annealing temperature on the morphology of the printed PSNs for a PS:PMMA weight ratio of 20:80. AFM images of the printed films are obtained after annealing at different temperatures (a) 200 °C, (b) 250 °C and (c) 300 °C for 5 min and after the selective development of the PS (left) or of the PMMA (center) phase. The scale bar represents 3 μm, and the corresponding 1D line profiles are shown on the right side.

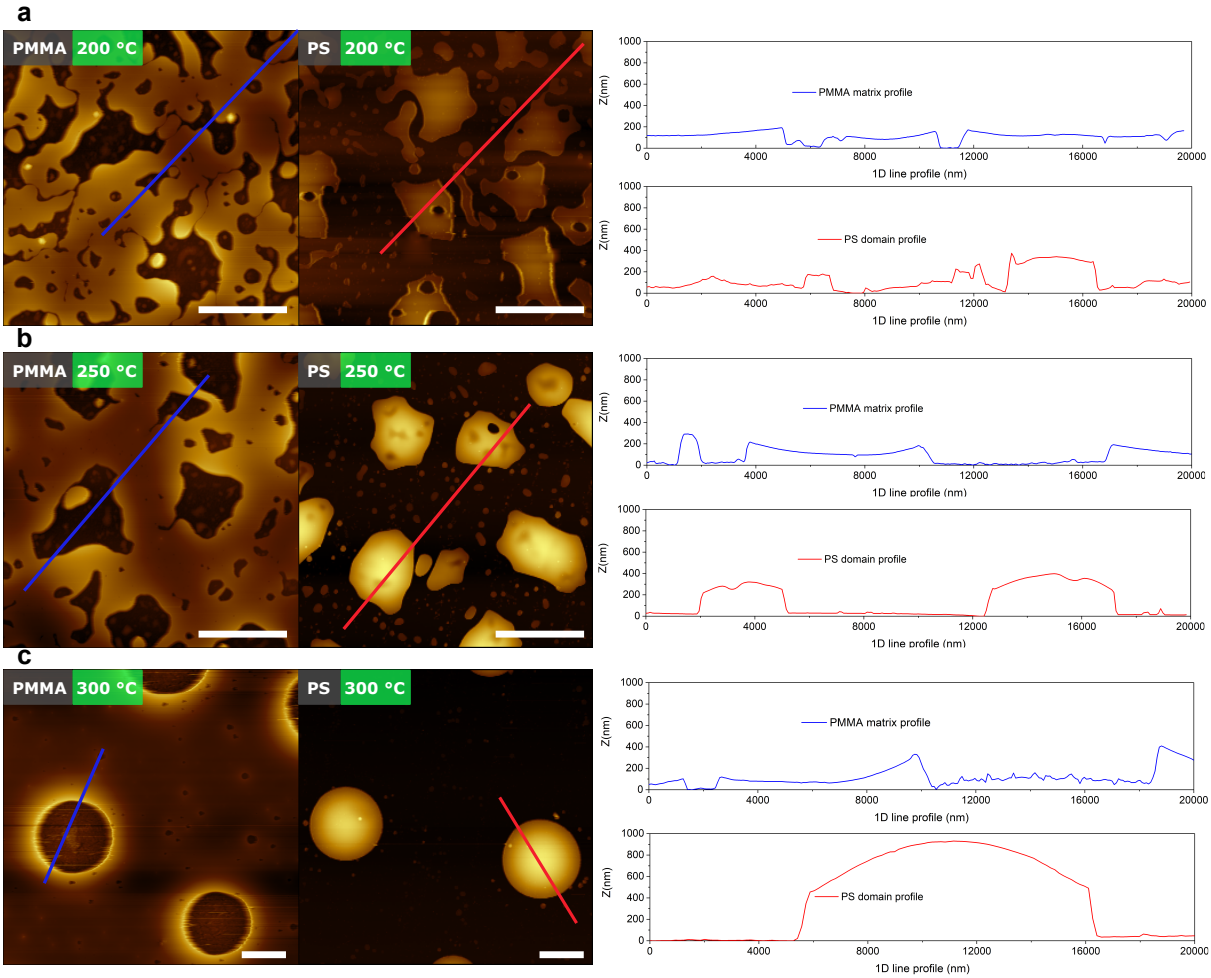

Figure S9. Influence of the annealing temperature on the morphology of the printed PSNs for a PS:PMMA weight ratio of 40:60. AFM images of the surface morphology obtained after annealing thin films at different temperatures (a) 200 °C, (b) 250 °C and (c) 300 °C for 5 min and selective development of PS (left) and PMMA (middle). The corresponding 1D line profile (right) to show the height change with annealing temperature. The scale bar represents 6 μm.

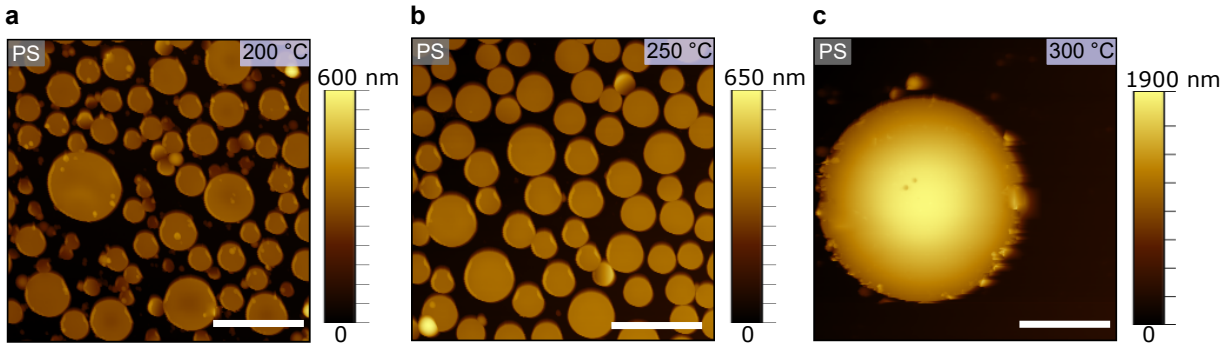

Figure S10. Influence of the annealing temperature on PSNs for a film printed with 1000 dpi. AFM images of the surface morphology obtained after annealing PS:PMMA films at different temperatures (a) 200 °C, (b) 250 °C and (c) 300 °C for 5 min and selective development of PMMA. The scale bar represents 3 μm in (a) and (b), and 9 μm in (c).

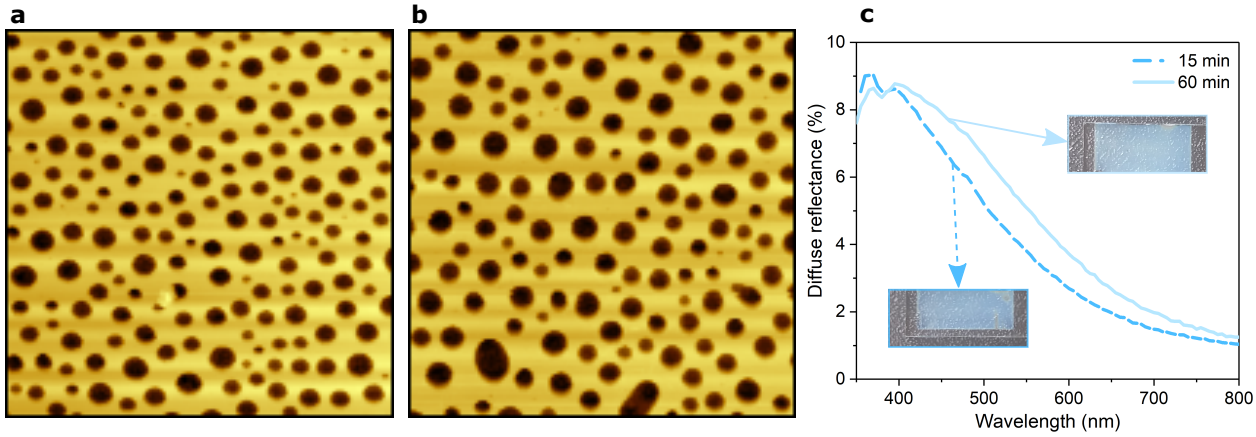

Figure S11. Influence of the annealing duration on the morphology of the printed PSNs for a film printed with 550 dpi. AFM images (5 μm $\times$ 5 μm) of the surface morphology obtained after annealing PS:PMMA (30:70) films at 150 °C for different durations (a) 15 min, (b) 60 min. (c) Corresponding diffuse reflectance spectra measured in samples annealed for 15 min and 60 min (cropped photographs of the samples shown as insets).

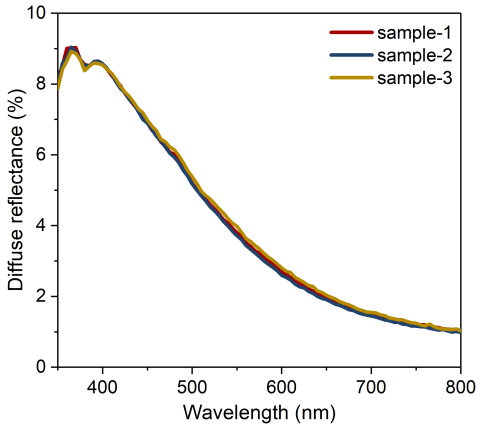

Figure S12. Optical properties of samples prepared at different days. Diffuse reflectance spectra of samples prepared using PS:PMMA (30:70) ink and with a printing resolution of 550 dpi.

Inkjet-printing of compact light extraction layers for OLEDs

To improve the outcoupling efficiency in an OLED (see **Figure S13**a), the introduced light extraction layer should efficiently scatter the trapped photons, and simultaneously allow a high optical transmittance. In other words, PSNs that are too scattering can be detrimental for the overall performance of the OLEDs and a trade-off between the two previously mentioned effects has to be found. To this end, the highly scattering printed sample shown in **Figure S13**b was exposed to an oxygen (O_2) plasma treatment to reduce the mean height of the PS nanopillars from 150 nm to 80 nm, resulting in a light extraction layer with a proper amount of light scattering (compare with the O_2 treated sample in **Figure 7**c). More precisely, the measured optical properties of the PS nanopillar arrays printed on a glass substrate, reported in **Figure S13**c, are as follows: light scattering coefficient (haze) of 4.6% and total transmittance (T-total, *i.e.* the sum of the diffuse and direct transmittance) of 89% at the OLED peak emission wavelength (λ_{peak}= 520 nm) for the O_2 treated sample (**Figure 7**c); and a higher haze of 18.3% as well as a lower T-total value of 82% for the untreated sample (**Figure S13**b). In addition to improving the haze with respect to the outcoupling efficiency, PS nanopillars with a lower aspect ratio and a smoother vertical profile, as obtained after the O_2 plasma treatment, also enable a conformal deposition of the OLED thin film stack atop the light extraction layer, leading to functional and reproducible devices. The exact morphology of the different interfaces in the OLED stacks was reproduced in the 3D model using the approach described in Ref.,[6] which exploits the surface morphology of the NPs and the layer thickness as input data. It was obtained by first extracting, using AFM, the topology of the phase-separated NPs (as shown in **Figure 7**b).

For OLEDs integrating the compact light extraction layer, the operating voltage is lower than that measured for the reference planar OLEDs (Reference OLED), which corresponds to an increased current density at the same bias voltage (see **Figure S13**d). This can be explained by the increased surface area of the ITO electrode upon the introduction of the PS nanopillar array.

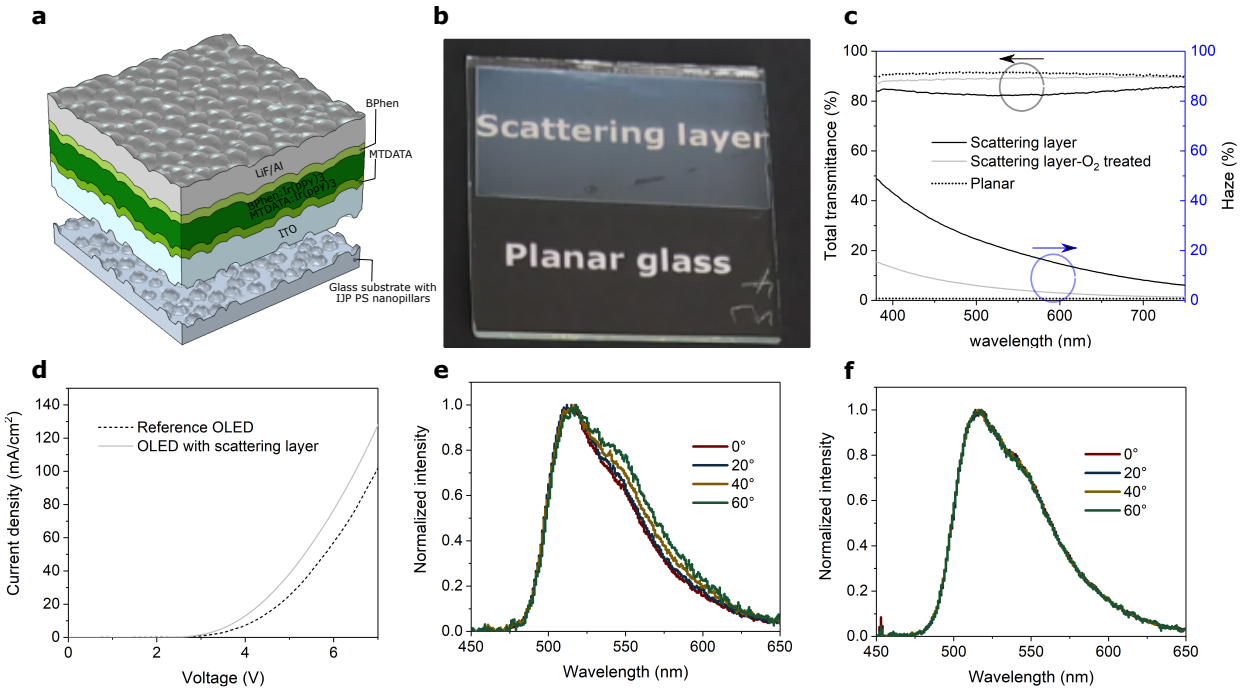

Figure S13. Optical properties of the standalone IJP light extraction layers and their performance after integration in OLEDs. a) 3D representation of the OLED stack grown on the compact light extraction layer (based on measured AFM scan) using the model described in Ref.[6] b) Photograph of a glass substrate, half-covered by the light scattering layer made of PS nanopillars (average height of 150 nm) after selective development of the PMMA phase from the PS:PMMA (30:70) thin film annealed at 200 °C and before O_2 plasma treatment. c) Total transmittance and haze of the glass substrates with the IJP scattering layer before and after O_2 plasma treatment, compared to a pristine glass substrate (planar). d) Current density *versus* voltage of the devices. (e)-(f) Goniometric measurements of the devices normalized spectra at angles between 0°and 60° for (e) reference OLED, and (f) OLED with scattering layer.

Figure S13e,f shows the angular emission behavior for an OLED with and without light scattering layer. It demonstrates that the presence of IJP PSNs can reduce the spectral shift observed in planar devices with increasing emission angles, which is attributed to weak microcavity effects.

References

(1) Huang, C. *Phase Separation in Thin Polymer Films: From Self-Stratification to Polymer Blend Lithography*, 1st ed.; Technische Universität Darmstadt: Darmstadt, **2015**; pp 1–135.

(2) Geveke, D. J.; Danner, R. P. Ternary Phase Equilibria of Polystyrene with a Second Polymer and a Solvent. *J. Appl. Polym. Sci.* **1993**, *47*, 565–575.

(3) Lau, W. W.; Burns, C. M.; Huang, R. Y. Interaction Parameters in Mixtures of Polystyrene-Poly (methyl Methacrylate)-Toluene. *Eur. Polym. J.* **1987**, *23*, 37–39.

(4) Huang, C.; Moosmann, M.; Jin, J.; Heiler, T.; Walheim, S.; Schimmel, T. Polymer Blend Lithography: A Versatile Method to Fabricate Nanopatterned Self-Assembled Monolayers. *Beilstein J. Nanotechnol.* **2012**, *3*, 620–628.

(5) Ougizawa, T.; Walsh, D. J. Upper Critical Solution Temperature Behavior in Polystyrene/Poly (methyl Methacrylate) Mixture. *Polym. J.* **1993**, *25*, 1315–1318.

(6) Jovanov, V.; Xu, X.; Shrestha, S.; Schulte, M.; Hüpkes, J.; Zeman, M.; Knipp, D. Influence of Interface Morphologies on Amorphous Silicon Thin Film Solar Cells Prepared on Randomly Textured Substrates. *Sol. Energy Mater. Sol. Cells* **2013**, *112*, 182–189.